

# Nanoscale

Accepted Manuscript



This is an *Accepted Manuscript*, which has been through the Royal Society of Chemistry peer review process and has been accepted for publication.

*Accepted Manuscripts* are published online shortly after acceptance, before technical editing, formatting and proof reading. Using this free service, authors can make their results available to the community, in citable form, before we publish the edited article. We will replace this *Accepted Manuscript* with the edited and formatted *Advance Article* as soon as it is available.

You can find more information about *Accepted Manuscripts* in the [Information for Authors](#).

Please note that technical editing may introduce minor changes to the text and/or graphics, which may alter content. The journal's standard [Terms & Conditions](#) and the [Ethical guidelines](#) still apply. In no event shall the Royal Society of Chemistry be held responsible for any errors or omissions in this *Accepted Manuscript* or any consequences arising from the use of any information it contains.

## ARTICLE

# Ambient-Processable, Printable Cu Electrodes for Flexible Device Applications: Structural Welding on a Millisecond Timescale of Surface Oxide-Free Cu Nanoparticles

Cite this: DOI: 10.1039/x0xx00000x

Received 00th January 2012,  
Accepted 00th January 2012

DOI: 10.1039/x0xx00000x

www.rsc.org/nanoscale

Sang-Jin Oh,<sup>a,§</sup> Yejin Jo,<sup>a,§</sup> Eun Jung Lee,<sup>a</sup> Sun Sook Lee,<sup>a</sup> Young Hun Kang,<sup>a</sup> Hye-Ji Jeon,<sup>b</sup> Song Yun Cho,<sup>a</sup> Jin-Seong Park,<sup>b</sup> Yeong-Hui Seo,<sup>a</sup> Beyong-Hwan Ryu,<sup>a</sup> Youngmin Choi,<sup>a,\*</sup> Sunho Jeong<sup>a,\*</sup>

Recently, various functional devices based on printing technologies have been of paramount interest, owing to their characteristic processing advantages along with excellent device performance. In particular, printable metallic electrodes have drawn attention in a variety of optoelectronic applications; however, research into printable metallic nanoparticles has been limited mainly to the case of environmentally stable Ag phase. Despite its earth-abundance and highly conductive nature, the Cu phase, to date, has not been exploited as an ambient-processable, printable material due to its critical oxidation problem in air. In this study, we demonstrate a facile route to generating highly conductive, flexible Cu electrodes in air by introducing the well-optimized photonic sintering at a timeframe of  $10^{-3}$  sec, at which the photon energy, rather than conventional thermal energy, is instantly provided. It is elucidated how the surface oxide-free, printed Cu particulate films undergo chemical structural/microstructural evolution depending on the instantly irradiated photon energy, and a successful demonstration is provided of large-area, flexible, printed Cu conductors on various substrates including polyimide (PI), polyethersulfone (PES), polyethylene terephthalate (PET), and paper. The applicability of the resulting printed Cu electrodes is evaluated via implementation into both flexible capacitor devices and indium-gallium-zinc oxide (IGZO) flexible thin-film transistors.

## Introduction

In the last decade, the technical demand for cost-effective, highly conductive patterned structures has tremendously increased in various fields of printed optoelectronics.<sup>1-4</sup> Among the variety of conducting building-block materials, including organometallic precursors, polymers, and metals, Au and Ag nanoparticles (NPs), which can be readily prepared in the form of printable liquid phase, have been widely studied.<sup>5,6</sup> However, the issue of the material cost of noble metal-based nanoparticles has been gradually addressed, and this issue must be resolved for the realization of practical, large-area, low-cost printed devices. One alternative is much cheaper Cu nanoparticles with the high conductivity comparable to those of Au and Ag nanoparticles. A critical challenge in any attempt to utilize Cu nanoparticles is the significant difficulty in synthesizing them in highly pure metal phase, unlike the case of noble metals, owing to the thermodynamical stability of the  $\text{Cu}_x\text{O}$  phase.<sup>7,8</sup> The presence of an oxide layer on the surface of Cu nanoparticles not only deteriorates the electrical conductivity of nanoparticle-derived patterned structures, but also increases the

onset annealing temperature for triggering atomic diffusion at interparticle junctions;<sup>8</sup> thus, the oxide layer-involved Cu nanoparticles allow for the generation of conductive Cu features only on expensive, high temperature-endurable substrates. In addition, in order to prevent the additional formation of oxide phase, an inert gas must be supplied during the annealing process for a long period of time; this restricts the practical applicability of these particles in ambient atmosphere-processable, high-throughput printed electronics. The practical requisites for Cu nanoparticles, which should be resolved in printed electronics, are as follows: (i) oxide-free starting materials for high conductivity, (ii) a low-temperature annealing process compatible with cheap, vulnerable PET and paper substrates, and (iii) processibility in air in a very short time in order for particles to be applied to a high throughput roll-to-roll process.

Recently, it has been demonstrated that the instant supply of photon energy, based on either a laser or a flash light, in air can generate highly conductive metal layers on flexible substrates,<sup>9-18</sup> the practical potential of this process was demonstrated by its implementation in a roll-to-roll process.<sup>14</sup> In particular, while

laser sintering is activated in spatially-limited areas with sophisticated optical systems, flash light based photonic sintering can be carried out with a large light-source loaded in a simple equipment geometry. However, to date, the successful demonstration of flash light sintering has been mainly fulfilled with easily-processable Ag nanoparticles that do not experience significant oxidation problems. Cu nanoparticle-derived conductive structures were achievable only with a polyimide film as a flexible substrate, not with cost-effective, transparent substrates with low glass transition temperatures, because of the necessity of excessive photon energy.<sup>15-18</sup> In a case in which an oxide phase is involved in Cu nanoparticles, additional energy should be supplied in order to produce the photo-chemical reduction of the oxide phase into pure Cu phase under the presence of a reducing agent, together with a threshold energy input for the structural densification. This results in a critical limitation in using vulnerable plastic substrates that undergo morphological deformation during irradiation by highly intensive photons. Most importantly, to date, no practical use for photo-sintered, printed Cu features has been suggested for flexible devices.

In this study, we demonstrate, for the first time, Cu nanoparticle-derived printed conductive structures on polyimide (PI), polyethersulfone (PES), polyethylene terephthalate (PET), and paper substrates using instant flash photonic sintering in air for completely surface oxide-free Cu nanoparticles. It is revealed that the combinatorial approach based on both oxide-free Cu nanoparticles and flash photonic sintering allows the possibility of resolving all requisites for conductive metal structures in printed flexible electronics; we also demonstrate that the suggested methodology can be used in flexible capacitor and thin-film transistor devices.

## Experimental

**Preparation of surface-oxide free Cu nanoparticle ink:** All chemicals were used as received without further purification. Cu acetate ( $\text{Cu}(\text{CO}_2\text{CH}_3)_2$ , 98%), octylamine ( $\text{C}_8\text{H}_{17}\text{NH}_2$ , 99%), oleic acid ( $\text{C}_{18}\text{H}_{34}\text{O}_2$ , 90%), phenylhydrazine ( $\text{C}_6\text{H}_5\text{NHNH}_2$ , 97%), and toluene ( $\text{C}_6\text{H}_5\text{CH}_3$ , anhydrous, 99.8%) were purchased from Aldrich. Cu nanoparticles were synthesized via chemical reduction of Cu ions in octylamine under inert atmosphere, as described in our previous study.<sup>19</sup> Briefly, 10.4 g of Cu acetate and 25.1 g of oleic acid were added to a three-neck round-bottomed flask containing 73.6 mL of octylamine. The oleic acid was incorporated as a surface capping molecule and phenylhydrazine was used as a reducing agent. The flask was fitted with a reflux condenser and a mechanical stirrer. The solution was purged with nitrogen for 60 min and then heated to 150 °C. Then, phenylhydrazine was added dropwise and the reaction was allowed to continue for 120 min. After completion of the synthesis reaction, the synthesized Cu nanoparticles were separated by centrifugation and washed with toluene. The synthesized Cu nanoparticles were kept in air without additional surface-passivation procedures. For the preparation of Cu conductive ink, the obtained Cu nanoparticles were dispersed in toluene. The solid loading was 20 wt% in the case of ink for drop-casting. Then, the prepared inks were subjected to ball milling for 1 hr. For the case of air-brush printing, the ink was diluted with more toluene to formulate the ink with a solid loading of 0.7 wt%.

**Air-brush printing and photonic sintering:** Air-brush printing was carried out on metal mask-loaded PI (thickness(t)

= 75  $\mu\text{m}$ , Kapton film 300HN, Teijin DuPont Films), PES (t = 120  $\mu\text{m}$ , Glastic SCL120, I-Components), PET (t = 125  $\mu\text{m}$ , Tetonon KEL86W, Teijin DuPont Films), and paper (basis weight = 251  $\text{g}/\text{m}^2$ , Premium photo paper semi-gloss, Epson) substrates using a commercially available pneumatic spray nozzle (Iwata, HP-SB) with an air back-pressure of 22 Pa. The distance between the substrate and the nozzle was 17 cm. The printing time was 23 sec while the knob was half open. The substrate temperature was kept to be 100 °C during air-brush printing. Photonic sintering was accomplished using a xenon flash lamp system (Sinteron 2010, Xenon Corp.) in which the A or B type lamp was equipped with a broadband spectrum of 370 to 800 nm or of 240 to 800 nm. The flash lamp dimensions were 0.8 cm in width and 40 cm in length, and the size of the moving stage was 900  $\text{cm}^2$ . In order to generate the electrical pulse energies, the air cooled xenon linear flash lamp, located 2 inches away from the substrate stage, delivered optical energy in a range from 0.39 to 2.44  $\text{J}/\text{cm}^2$ , as a function of the electrical voltage and the duration time. The optical energies of the flash lamp irradiation were measured using a radiometer (ITL1700, International Light Technologies) with a detector (SED033, 200-1100 nm, International Light Technologies). The substrate temperatures during photo-annealing were detected using a thermometer (1311A, K-Type, TES) and a thermo-indicator (3MC-40/55/70, AS TOOL).

**Fabrication of flexible capacitors and In-Ga-Zn-O (IGZO) thin-film transistors:** The flexible capacitors were fabricated by depositing Cu electrodes using air-brush printing technique and by spin-coating a 6  $\mu\text{m}$ -thick PDMS dielectric on the polymeric substrates of PET, PES, and PI. The bottom Cu electrodes were formed on lower polymeric substrates, followed by continuous photonic sintering with optimized conditions (2.3 kV for 1.5 msec for PET, 2.0 kV for 1.5 msec for PES, and 2.5 kV for 1.5 msec for PI). The moving speed of the stage was 300 mm/min and the pulse on/off time was 1.5/998.5 msec. Then, a mixture of PDMS precursor, curing agent (Sylgard 184, Dow Corning Corp.), and hexane at a ratio of 10:1:6 (w/w) was spin-coated on top of the Cu electrodes and dried at 60 °C for 4 h. For electrical measurements, Au wire (diameter = 0.5 mm, Alfa Aesar) was connected to each Cu electrode using a silver paste (CW-2400, Chemtronics) and dried at 80 °C for 10 min. On the upper polymeric substrates, top Cu electrodes were air-brush printed and photo-sintered with the conditions same as the case of bottom electrodes. In order to make a firm contact between the lower and upper substrates, both substrates in the contact were placed in a vacuum chamber with a pressure of 76 cmHg. The active area of the metal-insulator-metal capacitors was 0.014  $\text{cm}^2$ . Flexible IGZO transistors were fabricated by depositing  $\text{Al}_2\text{O}_3$  (thickness (t)= 40 nm), ITO (thickness (t)= 100 nm),  $\text{Al}_2\text{O}_3$  (thickness (t)= 100 nm), and IGZO (thickness (t)= 30 nm ) layers on 75  $\mu\text{m}$ -thick polyimide-coated glass substrates, followed by annealing at 200 °C. ITO and IGZO layers were deposited by sputtering;  $\text{Al}_2\text{O}_3$  layer was deposited using the atomic layer deposition method. The Cu source/drain electrodes, with channel dimensions of 60  $\mu\text{m}$  in length and 1000  $\mu\text{m}$  in width, were air-brush printed on top of the prepared IGZO/ $\text{Al}_2\text{O}_3$ /ITO/ $\text{Al}_2\text{O}_3$ /PI/glass substrates; they were then photo-sintered at 2.0 kV for 1.5 msec. As a control sample, printed Cu electrodes were heat-treated with a rapid thermal annealing (RTA) system, with a heating rate of 200 °C/min, at 350 °C for 15 min. For cases in which RTA was carried out at temperatures below 350 °C or for times shorter than 15 min, the

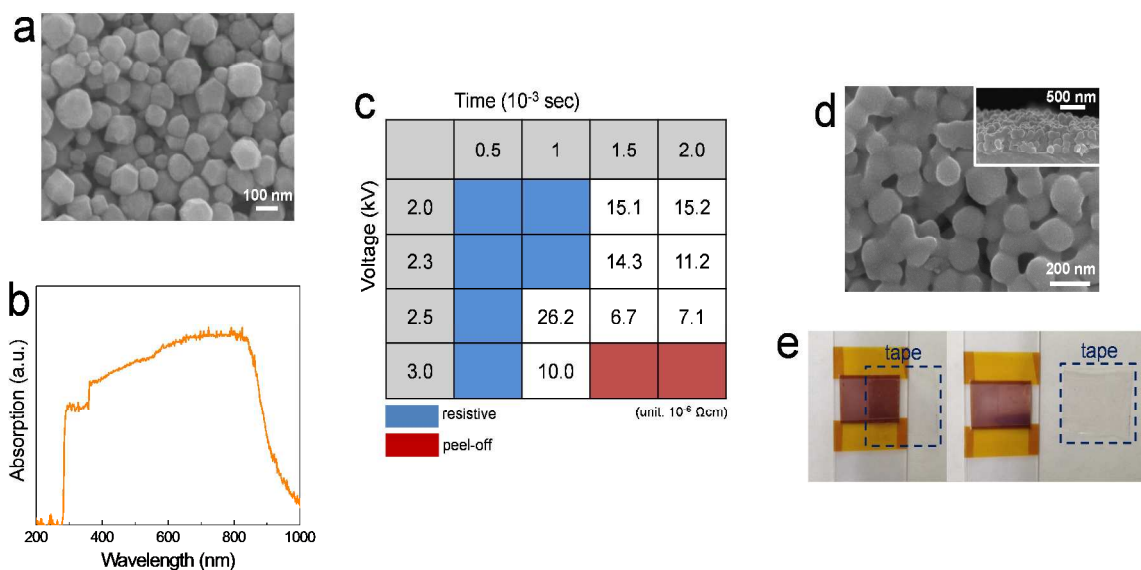


Figure 1. (a) SEM image and (b) UV-visible spectrum for surface oxide-free Cu nanoparticles. (c) Resistivity evolution of air brush-printed Cu nanoparticle layers depending on the photon generation conditions, voltage and duration time. (d) SEM image and (e) adhesion test result for Cu conductive layer photo-sintered at 2.5 kV for 1.5 msec. All Cu films were prepared by air-brush printing on polyimide substrates.

Cu electrodes were highly resistive due to the insufficient structural densification. The final devices were detached manually from the glass substrates.

**Characterization:** The size and shape of the synthesized Cu nanoparticles, and the microstructures of the Cu conductive layers, were examined by scanning electron microscopy (SEM, JSM-6700, JEOL). The crystal structure of the Cu nanoparticles was analyzed using an X-ray diffractometer (XRD, D/MAX-2200V, Rigaku). Chemical structural analysis of the Cu nanoparticles/layers was performed with X-ray photoelectron spectroscopy (XPS, K-Alpha, Thermo Fisher Scientific). The absorption spectra for the Cu nanoparticle ink were measured using UV-Vis spectroscopy (UV-2501PC, 200-1100 nm, Shimadzu). The resistivity of the Cu conductive layers was analyzed using a four point probe (FPP-HS8, Dasol Eng.) with a bending machine (PMC-1HS, Autonics) under a bending radius of 7 mm. The capacitance and leakage current of the flexible capacitor devices were measured using a precision impedance analyzer (Agilent, 4294A) and a semiconductor parameter analyzer (Agilent, 4155C), respectively, with a corresponding bending machine under a bending radius of 7 mm. The transfer characteristics of the transistors were analysed with an Agilent E5272 semiconductor parameter analyzer. All electrical measurements were performed in the dark under ambient conditions.

## Results and Discussion

The surface oxide-free Cu nanoparticles were synthesized through a chemical reduction of Cu ions with a reducing agent, phenylhydrazine, under the presence of oleic acid acting as a capping molecule, as reported in our previous work.<sup>19</sup> Cu nanoparticles with a bimodal size distribution below 100 nm were synthesized (Figure 1a); the phase purity, not accompanied with any secondary phases, was confirmed by X-ray diffraction (XRD) and X-ray photoelectron spectroscopy

(XPS) Cu  $2p_{3/2}$  spectrum (Figure S1). Owing to the characteristic oxide-free surface structure, it was possible to use conventional thermal annealing to transform the Cu nanoparticle layers into highly conductive bulk-like films with a low resistivity of  $5.9 \mu\Omega \cdot \text{cm}$ , comparable to that of pure bulk material, at relatively low temperatures (Figure S2). However, even with surface oxide-free Cu nanoparticles, annealing at over  $300^\circ\text{C}$ , a process not compatible with cost-effective plastic substrates, was still required to evolve highly conductive structures under an inert atmosphere without the involvement of chemically active environments such as  $\text{H}_2$  or carboxylic acids. Figure 1b shows the UV-visible spectra for the Cu nanoparticle colloidal fluid; these spectra were measured to evaluate how effectively the Cu nanoparticles absorb the flash light ranging in wavelength from 240 to 800 nm. It was revealed that the photons in the overall range between 270 and 830 nm are absorbed, from which it was expected that photon energy instantly irradiated from a flash lamp could act as another source to replace conventional thermal heat.

First, in order to elucidate the influence of photonic sintering on the various reactions inside the Cu nano-particle films without the limitation of polymeric substrates, air-brush printed Cu layers were formed on polyimide (PI) substrates, followed by photonic sintering in air under different processing conditions. As can be seen in Figure 1c and d, the insulating Cu particulate films were gradually converted into conductive films with well-interconnected conductive pathways, depending on the processing parameters, the electrical voltage and the duration time, to generate photons from the lamp. The photon dose and the substrate temperature as functions of the voltage and time are summarized in Figure S3. It should be noted that the substrate temperature did not exceed  $110^\circ\text{C}$  for all processing conditions, owing to the transfer of thermal energy, which was derived from the dissipation of photons inside the inorganic matrix, into the Cu layers and the instant heat release outward to the ambient; this implies that the photonic sintering process, based on surface oxide-free Cu nanoparticles, can be

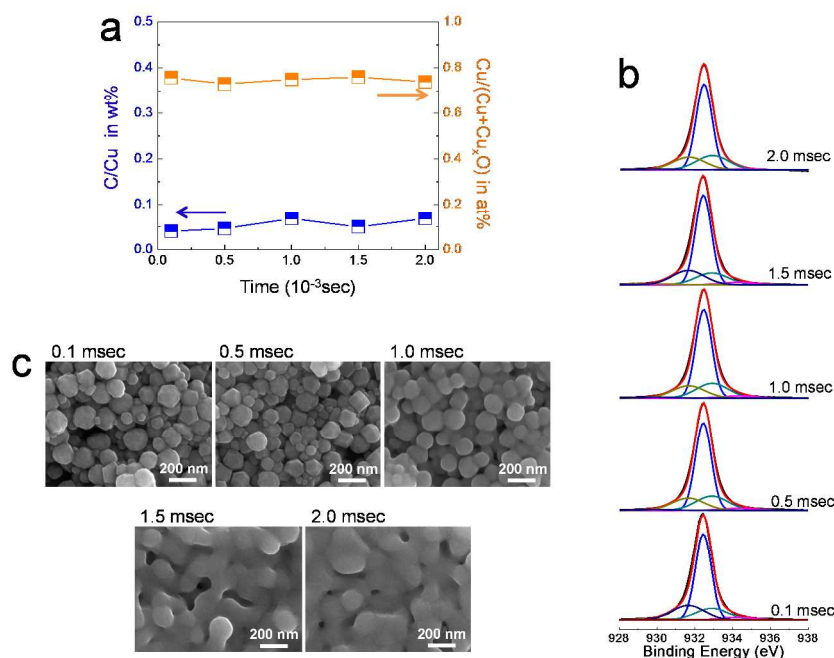


Figure 2. (a) Compositional variation in C/Cu weight ratio and chemical structural variation in Cu/(Cu+Cu<sub>x</sub>O) atomic ratio. (b) XPS Cu 2p<sub>3/2</sub> spectra and (c) SEM top-view images for Cu nano-particulate films photo-sintered at 2.5 kV for different duration times ranging from 0.1 to 2.0 msec. All Cu films were prepared by air-brush printing on polyimide. Prior to XPS analysis, all samples were etched for 390 sec to get rid of contaminated surfaces.

compatible with plastic substrate-based flexible electronics. A low resistivity of 6~7 μΩ·cm, almost corresponding to the resistivity of thermally-driven Cu nanoparticle layers, was obtained after photonic sintering at 2.5 kV for 1.5-2.0 msec. In this study, a 75 μm-thick film was used as a substrate; in some studies, to prevent the polymer substrate from deforming under the irradiation of highly energetic photons, thicker polymeric substrates were employed. It was observed that the highly conductive Cu films adhere well to PI substrates without delaminating from the substrates even after a firm adhesion test using the adhesive tape used in the ASTM 3359 method (Figure 1e). Under processing conditions of 3.0 kV for times longer than 1.5 msec, the film peeled off completely from the substrates due to photo-chemical damage on the underlying PI substrates (Figure S4). A substrate temperature below 110 °C indicates that the photo-chemical damage is a dominant factor over the thermal degradation of the PI substrate itself. In the case of the irradiation of photons with a wavelength between 370 and 800 nm, the Cu films did not peel off at condition of 3.0 kV and 1.5 msec; this is also indicative of the dominant impact of photo-chemical damage on underlying substrates. The dependency of the resistivity evolution on photonic sintering conditions in air-brush printed films was similar to that observed in drop-casted films, as shown in Figure S5. This implies that the Cu nanoparticle assemblies in air-brushed films are well-packed enough not to adversely affect the interparticular growth or, in turn, the resistivity evolution.

The chemical structural, and microstructural transformations during photonic sintering were further investigated for Cu layers photo-sintered at 2.5 kV for different timeframes ranging from 0.1 to 2.0 msec. Figure 2a shows the variations in C/Cu and Cu/(Cu+Cu<sub>x</sub>O) ratios depending on the duration time. The data was acquired from XPS spectra for

samples pre-etched for 390 sec, and the ratios of Cu/(Cu+Cu<sub>x</sub>O) were obtained through areal integration-based semi-quantitative calculations for each sub-peak in the Cu 2p<sub>3/2</sub> spectra. All XPS Cu 2p<sub>3/2</sub> spectra are shown in Figure 2b. The peaks positioned at 932.5, 932.9, and 934.3 eV are attributable to Cu, Cu<sub>2</sub>O, and CuO, respectively. The peaks at 929.9 and 931.7 eV resulted from unknown phases, which might be associated with intermediate phases produced by the photo-chemical reaction between the Cu atoms and oxygen atoms of oleate anchored to the Cu nanoparticle surfaces. These unknown phases were also identified in the O 1s peak (Figure S6). The weight ratio of C/Cu for the as-prepared Cu nanoparticles was 0.13. It was observed that the content of residual carbon decreases significantly to 0.04 upon irradiation of intensive light for even 0.1 msec; this did not vary during photonic sintering for more prolonged duration times. This indicates that the surface capping organic moieties, which significantly hinder the interparticular atomic migration,<sup>20,21</sup> can be removed effectively through instant photon irradiation even at a timescale of 10<sup>-4</sup> sec; thus, it is presumed that the residual carbon content is not a predominant determining factor in the resistivity evolution. Similarly, the fractions of oxide inside the photo-annealed Cu layers were not found to vary at all, regardless of the duration time, at 2.5 kV, except for the fact that subtle oxidation took place with an atomic fraction of ~0.75. It should be noted that the photonic sintering in this study was carried out in air without provision of any inert gas or vacuum environment, unlike the cases of widely-reported conventional thermal annealing studies.<sup>7,8,22,23</sup>

As is well known, the pure copper phase must undergo the oxidation reaction into either CuO or Cu<sub>2</sub>O even at moderately elevated temperatures in air. For organic molecule-capped Cu nanoparticles, the oxidation can be suppressed through an effective passivation by densely-packed surface capping

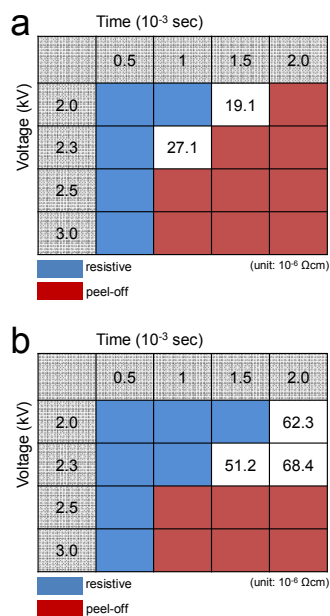


Figure 3. Resistivity evolution of Cu nanoparticle layers air brush-printed on (a) PES and (b) PET substrates, depending on the photon generation conditions, voltage, and duration time.

molecules; however, the removal of the capping molecules in air to trigger mass transport-based microstructural densification gives rise to the significant possibility of a thermodynamically driven, vigorous surface-to-bulk oxidation reaction, resulting in insulating, black-colored  $\text{Cu}_x\text{O}$  phases. This necessity of controlled atmospheres is a heretofore unresolved critical drawback in replacing Ag nanoparticle electrodes with cost-effective Cu nanoparticle-based alternatives in various practical applications. For the case of the photonic sintering process, the formation of a bare surface by photo-chemical partial removal of capping layers and the subsequent structural transformation into bulk phase occur almost simultaneously at a timescale of  $\sim 10^{-3}$  sec. The instantly transformed, three dimensionally-interconnected structures, with a very small volumetric fraction of void, behave in a manner similar to that of the bulk Cu layer, in which the surface oxidation, restricted to a thickness of a few nanometers, takes place only below  $150^\circ\text{C}$ . The temperature did not exceed  $150^\circ\text{C}$  during photonic sintering at 2.5 kV. This kinetically-suppressed oxidation inside the Cu nanoparticle-derived electrode architectures resulted in slightly oxidized Cu structures, along with the generation of highly conductive electrical properties.

As shown in Figure 2c, the predominant factor in determining the resistivity of photo-sintered Cu layers was the degree of microstructural evolution into bulk-like skeletons. For a duration time below 0.5 msec, local welding between neighboring nanoparticles was clearly observed; however, the generation of a bulk-like structure in a long-range order did not occur due to the insufficient supply of energy. It was revealed that the duration times for the on-set and for the completed long-range structural transformation were 1.0 and 1.5 msec, respectively, which values correspond well with the resistivity evolution depending on the duration time at 2.5 kV. The resistivity of  $6\sim 7 \mu\Omega\cdot\text{cm}$ , slightly higher than that of pure bulk Cu, was attributed to the presence of a subtle oxide phase and a small amount of voids. In previously reported Cu nanoparticles, the surface oxide phase drastically degraded the electrical

conductivities in thermally driven Cu nanoparticle conductors due to the inefficient mass transport in the oxide phases.<sup>8</sup> However, for the case of the Cu structures in this study, the additional subtle oxide phase formed together with a complete microstructural densification at a very short timescale; the subtle oxide phase slightly degraded the electrical resistivity, similar to the influence of the insulating air pores in the Ag nanoparticle-derived electrodes with resistivities of  $4\sim 10 \mu\Omega\cdot\text{cm}$ .

It is believed that the photo-sintered Cu electrodes behave like a conventional Cu foil, as they are composed of fully interconnected microstructure and the thermodynamically-driven surface oxidation occurs in a limited nanoscale. For clarifying it further, we compared the thermal stability of photo-sintered Cu electrodes with that of Cu foil, by measuring the resistivity as a function of annealing temperature. The annealing procedure was carried out for 1 hr in air. As seen in Figure S7, for photo-sintered Cu films, the resistivity started to increase above  $150^\circ\text{C}$ , and the color of films was changed after annealing at  $200^\circ\text{C}$ . This is attributed to the well-known, accelerated oxidation of Cu phase at elevated temperatures, which was confirmed with XRD results evolving the occurrence of  $\text{Cu}_2\text{O}$  phase. However, the identical thermal behavior is also observable for the case of conventional Cu foil; this indicates that the thermal stability of photo-sintered Cu films is analogous to that of Cu foil. Such a thermal instability at elevated temperatures is the inherent impediment for Cu-based electrodes. To date, the much effort has been devoted to improve the stability of Cu phase under various operating conditions by employing inorganic or organic passivating layers.<sup>24-28</sup> The exploit of various passivation layers suitable for photo-sintered Cu electrodes are prerequisite for further improving practical applicability.

Figure 3 shows the resistivity evolution of air-brush printed Cu particulate films on PES and PET substrates. The flash lamp light, in which ultraviolet light (UV) with wavelength below 370 nm is cut-off, was used to minimize the photo-chemical damage on the underlying vulnerable polymeric substrates. As seen in the energy dose for the visible flash lamp (Figure S8), the energy dose input diminished in the overall photon generating conditions, owing to the exclusion of highly energetic ultraviolet light. Under optimum conditions, a resistivity of  $19.1 \mu\Omega\cdot\text{cm}$  was found to evolve after photonic sintering at 2.0 kV for 1.5 msec for the case of the PES substrate, and a resistivity of  $51.2 \mu\Omega\cdot\text{cm}$  was measured after photonic sintering at 2.3 kV for 1.5 msec for the case of PET substrate. The slightly higher resistivities, compared with that of Cu electrodes on PI substrate, were attributable to the limited supply of photon energy in the UV cut-off flash lamp. The resistivity discrepancy between the Cu electrodes on the PES and PET substrates resulted from the greater heat dissipation due to the higher thermal conductivity of the PET substrate. However, these slightly high resistivities are still acceptable for printed electronics requiring Cu nanoparticle based conducting structures and, even such values as these, to date, have been not reported in the case of instant processing in air. For example, according to theoretical calculations,<sup>29</sup> 300 nm-thick patterns with resistivity of  $\sim 50 \mu\Omega\cdot\text{cm}$  allow for the generation of mesh structured transparent conductive films with transparency over 85 % and sheet resistance lower than  $10 \Omega/\text{square}$  for cases with an invisible linewidth of  $8 \mu\text{m}$  and a pitch length of  $100 \mu\text{m}$ , and for cases of a linewidth of  $40 \mu\text{m}$  and a pitch length of  $600 \mu\text{m}$ . Linewidths of 8 and  $40 \mu\text{m}$  are dimensions of patterned structures achievable by representative nozzle-jet

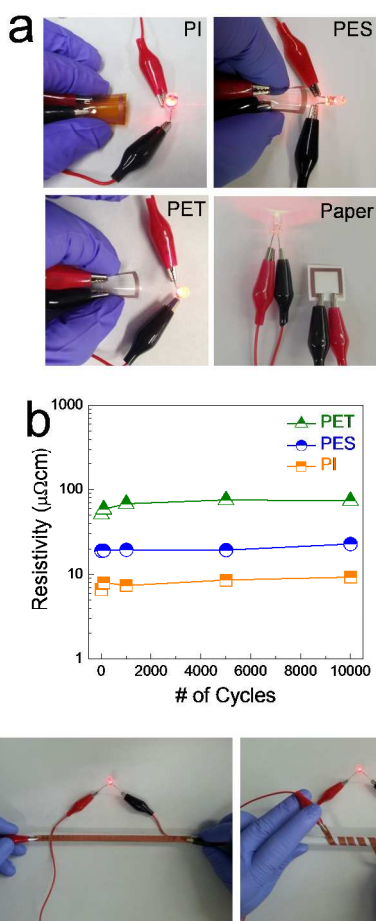


Figure 4. (a) Photographs for printed, conductive Cu patterns on PI, PES, PET, and paper substrates. (b) The resistivity variation as a function of bending cycles for printed, conductive Cu patterns formed on PI, PES, and PET substrates. The photonic sintering was carried out at 2.5 kV for 1.5 msec, at 2.0 kV for 1.5 msec, at 2.3 kV for 1.5 msec, and at 2.0 kV for 1.5 msec for the cases of PI, PES, PET, and paper substrates, respectively. (c) Photographs of 20 cm-long conductive Cu films prepared by continuous photonic sintering method.

(electrohydrodynamic-jet)<sup>29</sup> and roll (gravure off-set) printing techniques.<sup>30</sup> In addition, the narrow processing window, requiring a photon energy below  $1.55 \text{ J/cm}^2$  without the involvement of UV light, indicates the paramount importance of surface oxide-free nanoparticles in generating the conductive structure on transparent, vulnerable plastic substrates, because the surface oxide-involved starting Cu nanomaterials require higher energy input for photo-chemical reduction of the oxide phase, which indispensably results in the critical damage to the substrates. After photonic sintering under optimized conditions, Cu films were found to adhere well to both PES and PET films without further post-treatments or insertion of adhesive interlayers between the Cu layer and the substrate (Figure S9).

As can be seen in Figure 4a, the resulting air-brush printed, photo-annealed Cu architectures on PI, PES, PET, and paper substrates were active as flexible conductors. The Cu electrodes formed on a paper substrate after photonic sintering at 2.0 kV for 1.5 msec had a resistivity of  $26.8 \mu\Omega\text{-cm}$ . Figure 4b shows the flexibility of the photo-sintered Cu layers on each substrate

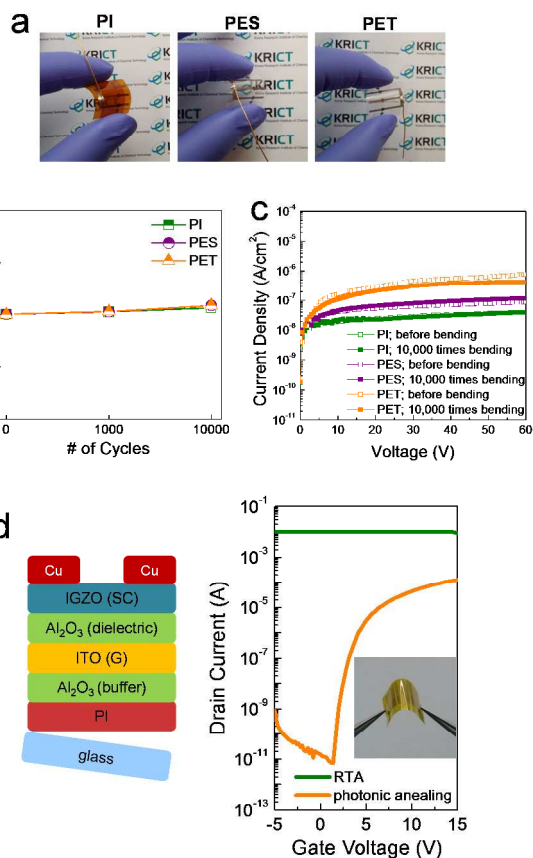


Figure 5. (a) Photographs, (b) variation of the normalized capacitance depending on the number of bending cycles, (c) leakage current behavior before/after 10,000 iterations of bending test for flexible capacitors employing the photo-sintered Cu electrodes. (d) Schematic diagram of flexible IGZO thin-film transistor and transfer characteristics for IGZO transistor employing RTA-treated and photo-sintered Cu electrodes. The SC and G in device structure implies the semiconducting layer and the gate electrode, respectively.

under 10,000 times-repeated bending tests. It was observed that the resistivity did not vary during extremely repeated conditions, only with a slight increment of resistivity in initial cycles. It is believed that the superior flexibility was achievable by the fully densified microstructure, rather than a particulate framework, along with the well-adhesive film properties on substrates. It is speculated that the initial increase of the resistivities resulted from the relaxation of structural stress inside films densified at very short time durations on the  $\sim\text{msec}$  scale. The significant processing advantage of the photonic sintering methodology is its facile accessibility to large-area roll-to-roll fabrications. Based on wet-phase nanoparticle inks, the predominant drawback in a roll-to-roll production of device-quality functional electrodes is the annealing step; conventional thermal annealing cannot be compatible with roll-to-roll processes, because an extremely long annealing zone should be involved to provide thermal energy for a prolonged time. In contrast, the instant irradiation of photons at a timescale of  $\sim\text{msec}$  enables the facile fabrication of nanoparticle-derived conductive metallic layers on a moving stage. As shown in Figure 4c, a highly flexible Cu conductive layer was formed on 20 cm-long substrates after photonic sintering for 40 sec. The

UV-visible lamp used was 40 cm in length and 0.8 cm in width. The pulse on and off time was 1.5 and 998.5 msec, respectively, and the stage moving speed was 300 mm/min.

Figure 5a shows the flexible capacitor devices composed of Cu bottom/top electrodes and PDMS dielectric on PET, PES, and PI substrates. The electrical properties of the resulting capacitor devices were measured in unbent state in air, after repeated bending tests for a specific number of cycles. As can be seen in Figure 5b and c, neither capacitance nor leakage current were found to vary significantly even up to 10,000-times cycles, indicating the complete flexibility/adhesive property of the Cu electrodes derived from nanoparticles on various polymeric substrates. Another interesting advantage of using photonic sintering for printed nanoparticulate Cu patterns is the capability of suppressing the significant diffusion of Cu atoms into other functional layers in multistacked device architectures. As a representative model study, we fabricated thin-film transistors (TFTs), on polyimide-coated glass substrates, by depositing air-brush printed Cu, ITO, Al<sub>2</sub>O<sub>3</sub>, and In-Ga-Zn-O (IGZO) layer as source/drain, gate, dielectric, and channel layer, respectively. The layers other than the Cu source/drain electrode were vacuum-deposited. In metal oxide-based transistors, copper is a promising conducting material as a source/drain electrode, owing to its low resistivity; however, in generating Cu source/drain electrodes, the vigorous diffusion of Cu atoms into the underlying layers and the formation of copper oxide in neighboring oxide channel layers have a critical adverse impact on device performance.<sup>31-33</sup> In particular, when nanoparticle-driven Cu patterned structures are thermally annealed in a conventional way to convert them into conductive electrodes, significant inward-diffusion of Cu atoms occurs inevitably because of the input of thermal energy for a prolonged time. As shown in Figure 5d, even using the rapid thermal annealing technique, the devices were entirely short-circuited in the overall gate-voltage range for device operation. In contrast, for the case of photonic sintering for the corresponding printed Cu patterns, it was clearly observed that the device was stably active, showing a field-effect mobility of 1.4 cm<sup>2</sup>/V·s and a threshold voltage of 1.2 V.

## Conclusions

In summary, we have demonstrated that highly conductive, flexible, printed Cu electrodes are attainable by adopting instant photonic sintering for surface oxide-free Cu nanoparticle assemblies, overcoming the previously reported difficulty in processing Cu nanoparticles in air. It was clarified that the surface oxide-free Cu nanoparticles underwent physical/chemical evolution in air as a function of incident photon energy, resulting in highly conductive, strongly adhesive Cu electrodes on PI, PES, and PET substrates. Resistivities of 6.7, 19.1, and 51.2 μΩ·cm were obtained in air for the photo-annealed Cu layers on PI, PES, and PET substrates, respectively, under optimized conditions. Also, the flexibility of the photo-annealed, printed Cu electrodes was demonstrated without any significant variation of resistivity, even after 10,000 cycle-bending tests on three different substrates. The possibility toward a roll-to-roll (R2R) process was suggested by the instant photonic sintering on a moving stage, allowing for the facile generation of 20 cm-long Cu electrodes. The potential accessibility for flexible device applications was demonstrated with flexible capacitor devices, and another interesting feature of photo-annealed Cu electrodes was verified with IGZO TFTs. It is believed that the scientific

findings suggested in this study, by resolving all heretofore recognized critical issues regarding the Cu phase in flexible printed device applications, would pave the way to facilitating ambient-processable, R2R process-compatible, high performance Cu electrodes.

## Acknowledgements

This research has been supported by the Korea Research Institute of Chemical Technology (KRICT) core project (KK-1402-C0) funded by the Ministry of Science, ICT and Future Planning.

## Notes and references

<sup>a</sup> Division of Advanced Materials, Korea Research Institute of Chemical Technology (KRICT), Daejeon 305-600, Republic of Korea

E-mail: youngmin@kRICT.re.kr (Y. Choi); sjeong@kRICT.re.kr (S. Jeong)

<sup>b</sup> Division of Materials Science and Engineering, Hanyang University Seoul, 133-719, Republic of Korea

<sup>†</sup>These authors contributed equally to this work.

Electronic Supplementary Information (ESI) available: X-ray diffraction result and XPS Cu 2p<sub>3/2</sub> spectrum for Cu nanoparticles, resistivity evolution in thermally treated Cu films, energy dose and intensity of flash lamps used in this study, SEM image for Cu films photo-sintered at 3.0 kV for 1.5 msec, resistivity evolution in photo-sintered, drop-casted Cu films, XPS O 1s spectrum for Cu film photo-sintered at 2.5 kV for 1.5 msec, adhesion test results for photo-sintered Cu films. See DOI: 10.1039/b000000x/

- 1 J. A. Rogers, *Nature*, 2010, **468**, 177.
- 2 N. S. Kim, K. N. Han, *J. Appl. Phys.*, 2010, **108**, 102801.
- 3 J. K. Hwang, S. Cho, J. M. Dang, E. B. Kwak, K. Song, J. Moon, M. M. Sung, *Nature Nanotechnol.*, 2010, **5**, 742.
- 4 B.-J. de Gans, P. C. Duineveld, U. S. Schubert, *Adv. Mater.*, 2004, **16**, 203.
- 5 J. Perelaer, M. Klokkenburg, C. E. Hendriks, U. S. Schubert, *Adv. Mater.*, 2009, **21**, 4830.
- 6 J. Perelaer, R. Jani, M. Grouchko, A. Kamyshny, S. Magdassi, U. S. Schubert, *Adv. Mater.*, 2012, **24**, 3993.
- 7 S. Jeong, H. C. Song, W. W. Lee, S. S. Lee, Y. Choi, W. Son, E. D. Kim, C. H. Paik, S. H. Oh, B. H. Ryu, *Langmuir*, 2011, **27**, 3144.
- 8 S. Jeong, K. Woo, D. Kim, S. Lim, J. S. Kim, H. Shin, Y. Xia, J. Moon, *Adv. Funct. Mater.*, 2008, **18**, 679.
- 9 J. Yeo, G. Kim, S. Hong, M. S. Kim, D. Kim, J. Lee, H. B. Lee, J. Kwon, Y. D. Suh, H. W. Kang, H. J. Sung, J.-H. Choi, W.-H. Hong, J. M. Ko, S.-H. Lee, S.-H. Choa, S. H. Ko, *J. Power Sources*, 2014, **246**, 562.
- 10 S. Hong, J. Yeo, G. Kim, D. Kim, H. Lee, J. Kwon, H. Lee, P. Lee, S. H. Ko, *ACS Nano*, 2013, **7**, 5024.
- 11 W. H. Chung, H. J. Hwang, S. H. Lee, H. S. Kim, *Nanotechnology*, 2013, **24**, 035202.
- 12 Y. Jo, S. Oh, S. S. Lee, Y.-H. Seo, B.-H. Ryu, Y. Choi, S. Jeong, *J. Mater. Chem. C*, 2014, **2**, 9746.
- 13 Y. Galagan, E. W. C. Coenen, R. Abbel, T. J. van Lammeren, S. Sabik, M. Barink, E. R. Meinders, R. Andriessen, P. W. M. Blom, *Organic Electron.*, 2013, **14**, 38.
- 14 M. Hösel, F. C. Krebs, *J. Mater. Chem.*, 2012, **22**, 15683.

- 15 B. Kang, S. Han, J. Kim, S. Ko, M. Yang, *J. Phys. Chem., C* 2011, **115**, 23664.
- 16 W. S. Han, J. M. Hong, H. S. Kim, Y. W. Song, *Nanotechnology*, 2011, **22**, 395705.
- 17 B. Y. Wang, T. H. Yoo, Y. W. Song, D. S. Lim, Y. J. Oh, *ACS Appl. Mater. Interfaces*, 2013, **5**, 4113.
- 18 W. S. Han, J. M. Hong, H. S. Kim, Y. W. Song, *Nanotechnology*, 2011, **22**, 395705.
- 19 S. Jeong, S. H. Lee, Y. Jo, S. S. Lee, Y.-H. Seo, B. W. Ahn, G. Kim, G.-E. Jang, J.-U. Park, B.-H. Ryu, Y. Choi, *J. Mater. Chem. C*, 2013, **1**, 2704.
- 20 S. Jeong, H. C. Song, W. W. Lee, Y. Choi, S. S. Lee, B.-H. Ryu, *J. Phys. Chem. C*, 2010, **114**, 22277.
- 21 S. Jeong, H. C. Song, W. W. Lee, Y. Choi, B.-H. Ryu, *J. Appl. Phys.*, 2010, **108**, 102805.
- 22 M. Grouchko, A. Kamyshny, S. Magdassi, *J. Mater. Chem.*, 2009, **19**, 3057.
- 23 K. Woo, Y. Kim, B. Lee, J. Kim, J. Moon, *ACS Appl. Mater. Interfaces*, 2011, **3**, 2377.
- 24 J. Song, J. Li, J. Xu, H. Zeong, *Nano Lett.*, 2014, **14**, 6298.
- 25 H.-G. Im, S.-H. Jung, J. Jin, D. Lee, J. Lee, D. Lee, J.-Y. Lee, I.-D. Kim, B.-S. Bae, *ACS Nano*, 2014, **8**, 10973.
- 26 I. N. Kholmanov, S. H. Domingues, H. Chou, X. Wang, C. Tan, J.-Y. Kim, H. Li, R. Piner, A. J. G. Zarbin, R. S. Ruoff, *ACS Nano*, 2013, **7**, 1811.
- 27 A. R. Rathmell, M. Nguyen, M. Chi, B. J. Wiley, *Nano Lett.*, 2012, **12**, 3193.
- 28 M. Grouchko, A. Kamyshny, S. Magdassi, *J. Mater. Chem.*, 2009, **19**, 3057.
- 29 Y. Jang, J. Kim, D. Byun, *J. Phys. D: Appl. Phys.*, 2013, **46**, 155103.
- 30 S. Jung, S. Lee, M. Song, D.-G. Kim, D. S. You, J.-K. Kim, C. S. Kim, T.-M. Kim, K.-H. Kim, J.-J. Kim, J.-W. Kang, *Adv. Energy Mater.*, 2014, **4**, 1300474.
- 31 J. S. Park, T. S. Kim, K. S. Son, E. Lee, J. S. Jung, K.-H. Lee, W.-J. Maeng, H.-S. Kim, E. S. Kim, K.-B. Park, J.-Y. Kwon, M. K. Ryu, S. Y. Lee, *Appl. Phys. Lett.*, 2010, **97**, 162105.
- 32 C.-K. Lee, S. Y. Park, H. Y. Jung, C.-K. Lee, B.-G. Son, H. J. Kim, Y.-J. Lee, Y.-C. Joo, J. K. Jeong, *Phys. Status Solidi*, 2013, **7**, 196.
- 33 W.-S. Kim, Y.-K. Moon, S. Lee, B.-W. Kang, T.-S. Kwon, K.-T. Kim, J.-W. Park, *Phys. Status Solidi*, 2009, **3**, 239.